Plasmoelectronic-Based Ultrasensitive Assay of Tumor Suppressor microRNAs Directly in Patient Plasma: Design of Highly Specific Early Cancer Diagnostic Technology

Thakshila Liyanage,[1] Adrianna N. Masterson,[1] Hector H. Oyem,[2] Hristos Kaimakliotis,[3] Hang Nguyen,[1] and Rajesh Sardar[,1,4]*

[1]Department of Chemistry and Chemical Biology, Indiana University-Purdue University Indianapolis, 402 N. Blackford Street, Indianapolis, Indiana 46202, United States

[2]School of Chemistry, Newcastle University, NE1 7RU, United Kingdom

[3]Department of Urology, Indiana University School of Medicine, 535 N. Barnhill Dr. Indianapolis, Indiana 46202, United States

[4]Integrated Nanosystems Development Institute, Indiana University-Purdue University Indianapolis, 402 N. Blackford Street, Indianapolis, Indiana 46202, United States

This is the author's manuscript of the article published in final edited form as:

Liyanage, T., Masterson, A. N., Oyem, H. H., Kaimakliotis, H., Nguyen, H., & Sardar, R. (2019). Plasmoelectronic-Based Ultrasensitive Assay of Tumor Suppressor microRNAs Directly in Patient Plasma: Design of Highly Specific Early Cancer Diagnostic Technology. Analytical Chemistry. https://doi.org/10.1021/acs.analchem.8b03768

ABSTRACT: It is becoming understood that microRNAs hold great promise for non-invasive liquid biopsies for screening for different types of cancer, but current state-of-the-art RT-PCR and microarray techniques have sensitivity limitations that currently restrict their use. Herein, we report a new transduction mechanism involving delocalization of photoexcited conduction electrons wavefunction of gold triangular nanoprism (Au TNP) in the presence of -ssDNA/microRNA duplexes. This plasmoelectronic effect increases the electronic dimension of Au TNPs and substantially affects their localized surface plasmon resonance (LSPR) properties that together allow us to achieve a sensitivity for microRNA assay as low as 140 zeptomolar concentrations for our nanoplasmonic sensors. We show that the position of a single base-pair mismatch in the -ssDNA/microRNA duplex dramatically alters the LSPR properties and detection sensitivity. The unprecedentedly high sensitivity of nanoplasmonic sensors has allowed us to assay four different microRNAs (microRNA-10b, -182, -143 and -145) from bladder cancer patient plasma (50 μL/sample). For the first time, we demonstrate the utility of a label-free, nanoplasmonic sensor in quantification of tumor suppressor microRNAs - the level of tumor suppressor microRNAs goes down in cancer patient as compared to normal healthy individuals - in metastatic and non-metastatic bladder cancer patient plasma. Our statistical analysis of patient samples unequivocally suggests that the tumor suppressor microRNAs are more specific biomarkers (p-value of <0.0001) than oncogenic microRNAs for differentiation between metastatic and non-metastatic bladder cancer, and non-metastatic cancer from healthy individuals. This work demonstrating the electron wavefunctions delocalization dependent ultrasensitive LSPR properties of noble metal nanoparticles has a great potential for fabrication of miniaturized and extremely powerful sensors to investigate microRNA properties in other cancers (for example breast, lung, and pancreatic) through liquid biopsy.

INTRODUCTION

In this article, we report the electron wavefunction delocalization process of metallic nanoparticles that results in dramatic alteration of the localized surface plasmon resonance (LSPR) properties of nanoplasmonic sensors with unprecedented sensitivity towards biomolecular recognition and quantification for the first time. Most importantly, assaying unmodified patient plasma using this fundamentally new transduction mechanism, we demonstrate that tumor suppressor microRNAs are more specific biomarkers than oncogenic microRNAs for differentiation between metastatic and non-metastatic bladder cancer (BC). MicroRNAs are small (18-25 nucleotides) single-stranded noncoding RNAs that, although targeting messenger RNAs, have the capacity to regulate multiple biological processes.1-4 Presently, the therapeutic potential of microRNAs is in its infancy,[5, 6] altered microRNA expression levels have been associated with a wide range of diseases[7-9] including cancer.1-4 Moreover, plasma microRNAs are found to be extremely stable under harsh conditions,[9] and so have a unique potential to serve as early diagnostic markers. BC represents the 4th most common malignancy diagnosed amongst males in the United States.[10] Currently, BC is under-staged in about 35% of

patients with clinical T2 muscle-invasive disease. At surgery, approximately 20% of this sub-population will also have metastatic nodal involvement and another 15% will have pathologic T3-T4 disease. Unfortunately, it is impossible to predict metastatic nodal disease during radical cystectomy in muscle-invasive BC patients using existing methods. The development of a highly accurate assay which can detect and monitor BC non-invasively through blood circulation (*"liquid biopsy")* would be highly beneficial for early diagnostic of BCs and will be the "holy grail" of urologic oncology.

Although oncogenic microRNAs – the level of oncogenic microRNAs goes up in cancer patient as compared to normal healthy individuals - can be quantified using various techniques directly from patient plasma,11-14 there is no report available in which tumor suppressor microRNAs are quantified using label-free techniques. Tumor suppressor microRNA levels decrease in cancer cells as compared to normal cells. Therefore, an ultrasensitive assay is required to quantify such changes. Herein, we report the construction of a solid-state nanoplasmonic sensor utilizing unique *"plasmoelectronic"* properties that is capable of detecting microRNAs (oncogenic microRNAs: microRNA-10b and -182; tumor suppressor microRNAs: microRNA-143 and -145) at zeptomolar (zM) concentrations directly from as low as 50 microliter (μL) of BC patient plasma with high specificity. Our technology obviates the complexity (reverse transcription, labeling, and amplification) and multiple time-consuming steps (treatment of the biological fluids and RNA extraction) associated with the existing real-time PCR and microarray-based microRNA quantification methods. We construct ultrasensitive gold triangular nanoprism (Au TNP)-based nanoplasmonic sensors by programmably controlling the structural parameters that influence the LSPR properties of TNPs. Our results show a nearly four and three orders of magnitude difference in concentrations between metastatic BC and normal control, and metastatic and non-metastatic BC, respectively, for tumor suppressor microRNA-143 and -145 with p-values of <0.0001. In contrast, less than 10-fold difference in concentrations are observed for the oncogenic microRNA-10b and -182.

EXPERIMENTAL SECTION

Materials. Chloro(triethylphosphine) gold (I) (Et_3PAuCl, 97%) was purchased from Gelest Inc, poly(methylhydrosiloxane) (PMHS, Mn = 1700-3300), trioctylamine (TOA, 98%), and ACS grade acetonitrile (CH_3CN, 99.9%) and methanol (99.8%) were purchased from Sigma Aldrich. Thiol modified 5'-SH-$(CH_2)_n$-ssDNAs and microRNAs were purchased from Integrated DNA Technologies (IDT). (3-mercaptopropyl)-triethoxysilane (MPTES, 94%) was purchased from Alfa Aesar. Ethanol (alcohol 200 proof) was purchased from Decon labs. Thiolated polyethylene glycols were purchased from purePEG. All the chemicals were used without any further purifications. RNase free sterile water was obtained from Baxter Healthcare Corporation. The glass coverslips were purchased from Fisher Scientific. RBS 35 Detergent was obtained from Thermo Scientific and used as received. Bladder cancer patient plasma samples were obtained from the Indiana University medical school and used as received. All water was purified using a Thermo Scientific Barnstead Nanopure system. Thiol modified -ssDNAs, microRNAs, and patient samples were stored at -80 °C. PBS buffer (pH = 7.2) was prepared using RNase free sterile water.

Preparation of nanoplasmonic sensors for microRNA assay. As developed by our laboratory, we performed a tape-cleaning procedure on the glass coverslip-attached Au TNPs to remove non-prismatic nanostructures.15, 16 Briefly, tape cleaning was performed by placing the adhesive scotch tape (3M corporation) onto the Au TNP-attached coverslips, gently pressed down with a finger, and then slowly removed at a 90° angle. The Au TNP-attached coverslips were then cut into four pieces using a diamond cutter. Au TNPs containing supporting substrates were then incubated into HS-$(CH_2)_n$-ssDNA-X: $SH\text{-}PEG_n$ (1 μM each) PBS buffer solution for overnight. Next, the -S-$(CH_2)_n$-ssDNA-X: -S-PEG_n-functionalized Au TNPs were rinsed with PBS buffer to remove loosely bound reactants that serve as nanoplasmonic sensors, which were further used for microRNA assay.

Development of microRNA calibration plots. The mixed -S–$(CH_2)_n$-ssDNA (n = 3, 6, and 9) and -S-PEG_n (n = 4 and 6) functionalized Au TNPs (nanoplasmonic sensors) were incubated in different concentrations (range 1.0 nM to 100.0 zM) of microRNA solution in 10 mL PBS buffer for overnight. MicroRNA-bound nanoplasmonic sensors were washed with PBS buffer to remove any nonspecifically adsorbed species, and then the LSPR extinction spectra were collected and λ_{LSPR} was determined. The calibration curves were plotted as $\Delta\lambda_{LSPR}$ (nm) verses logarithm concentration (nM). During the spectral collection the refractive index of the bulk medium kept constant by measuring all extinction spectra in PBS buffer.

Quantification of microRNA for bladder cancer patient samples. Nanoplasmonic sensors were incubated in a solution containing 50 □L of a bladder cancer patient sample (MT/ NMT/ Normal control samples) diluted into 3 mL PBS buffer for 12 h. Then the sensors were thoroughly washed with PBS buffer to remove any nonspecifically adsorbed biomolecules. Finally, the LSPR extinction spectra were recorded to determine λ_{LSPR}.

Fluorescence quantification of microRNA for different single base pair mismatches. An approximate concentration of microRNAs (fully complementary and having a single base-pair) attached onto the nanoplasmonic sensor were quantified by fluorescence spectroscopy using the procedure reported in the literature.[17] First, we prepared our nanoplasmonic sensors (HS–$(CH_2)_6$-ssDNA-10b and PEG_6-SH) as described above and then hybridized with target microRNAs. Here we used 1.0 nM solution of 5' FAM fluorophore-functionalized microRNA for the complementary (microRNA-10b), single base-pair mismatch (microRNA-p, microRNA-10a, and microRNA-q), and three starting nucleotides missing (microRNA-r). After the 12 h hybridization nanoplasmonic sensors with microRNAs, they were thoroughly rinsed with PBS buffer, and then incubated in aqueous 20 mM mercaptoethanol solution for the overnight ligand exchange reaction. The exchanged solution was collected and centrifuged at 10,000 rpm for 40 min. Then the solution part was carefully removed and

the solid (5' FAM fluorophore-functionalized microRNAs) was collected that was further dissolved in 1.5 mL of PBS buffer. Finally, photoluminescence spectra were collected.

Data processing and statistical analysis. The λ_{LSPR} was obtained by using maxima of the UV-visible extinction spectra determined from curve fitting using Origin software, and then $\Delta\lambda_{LSPR}$ was derived by taking the difference between LSPR peak of nanoplasmonic sensors before and after hybridization with target microRNA. Calibration curves were obtained by plotting $\Delta\lambda_{LSPR}$ vs. microRNA concentration. Finally, the LOD was determined by using z value (**mean+ 3σ, here σ is the standard deviation**), which was obtained from six $\Delta\lambda_{LSPR}$ measurements of the sensors incubated in buffer solution without microRNAs (blank). Concentration of target microRNAs in patient and normal control samples were determined from the calibration curves developed in human plasma (**see Table S7 and 8, and Figure S6**). We used six $\Delta\lambda_{LSPR}$ values and corresponding concentrations, and then the average concentration was calculated. Each patient sample was independently analyzed twice (two weeks apart).

RESULTS AND DISCUSSION

In principle, the working hypothesis of any nanoplasmonic sensors is heavily dependent on detecting changes in local dielectric environment.[16, 18-21] MicroRNAs with a single nucleotide difference in their sequence would expect to display nearly identical refractive indices, and thus the change in local dielectric environment of Au TNPs and LSPR response upon formation of -ssDNA/microRNA duplex should be nearly identical. Recently, we demonstrated that our nanoplasmonic sensors are capable of differentiating between microRNAs with single nucleotide specificity in the picomolar (pM) to femtomolar (fM) concentrations range. A fully complementary microRNA-10b and a single base-pair mismatch at the 12th position (microRNA-10a) provided limit of detections (LODs) of 32 aM and 0.15 pM, respectively.[15] We rationalized that the nearly 10^4 fold difference in sensitivity observed is a

consequence of delocalization of surface plasmon excitation of Au TNP into -ssDNA/microRNA duplex that alters the electronic dimension the TNPs through delocalization of excitonic wavefunctions, resulting in a variation of the LSPR properties. Furthermore, the single nucleotide specificity of our nanoplasmonic sensors is based on the excitonic wavefunctions delocalization mechanism, which provides variable magnitude of LSPR response for different microRNAs. This selectivity is different than the traditional biological assay in which stronger the interaction – a fully complementary –ssDNA/microRNA duplex should display stronger binding interaction than the –ssDNA/microRNA duplex containing nucleotide mismatches - between the receptor and analyte, higher is the signal and thus better is the selectivity. In this article, for the first time we examine the surface plasmon excitation delocalization mechanism by varying base-pair mismatch between -ssDNA and microRNA and controlling the distance between the surface of TNP and -ssDNA. Taken together, this unique electronic phenomenon, which has not been demonstrated before with respect to the characterization of LSPR-based transduction mechanisms, has allowed us to assay microRNA at ultra-low concentrations directly in unmodified BC patient plasma.

Controlling Surface Plasmon Excitation Delocalization by Varying Base-Pair Mismatch.

Delocalization of surface plasmon excitation (conduction electrons) of metallic nanoparticles is a steady-state electronic phenomenon in which wavefunctions of conduction electrons are expected to leave the metallic construct and expand into the surrounding environment, including into ligand moieties. When this occurs, the electron density around the nanoparticle reduces, resulting in the LSPR peak red-shifts.[22] **Figure 1A** shows the construction of our solid-state nanoplasmonic sensor using chemically-synthesized ~42 nm edge-length and ~8 nm width Au TNPs (**Figure 1B**) attached onto silanized glass substrates. Light irradiation onto TNP induces the collective oscillation of conduction electrons and creates the LSPR properties. The electron wavefunctions are then allowed to delocalize through a highly pi-stacked -ssDNA/microRNA duplex. Our hypothesis is that both the extent of

delocalization and the LSPR sensitivity will decrease upon presence of base-pair mismatches in the –ssDNA/microRNA duplex, where the largest reduction in LSPR sensitivity is expected to be observed when the mismatches are closest to the surface of the TNP. To investigate the effects of base-pair mismatch on wavefunction delocalization and the LSPR sensitivity of nanoplasmonic sensors, in the current work we select -ssDNA-10b as a model oligomer for the microRNA-10b recognition molecule. Sequences for other microRNAs are shown in **Figure 1C** and Supporting Information Tables (**Table-S1 and -S2**)

We measured LSPR response ($\Delta\lambda_{LSPR}$) of $-S(CH_2)_6$-ssDNA-10b-functionalized Au TNPs (nanoplasmonic sensor) after attachment of microRNAs as a function of concentration (1.0 nM to 100.0 aM) and location of single base-pair mismatch in PBS buffer (wet nanoplasmonic sensors). The detailed experimental procedure for the fabrication of nanoplasmonic sensors is provided in the Supporting Information. **Figure 2A** illustrates $\Delta\lambda_{LSPR}$ values (nm) for different microRNAs. Using our published procedure (see Supporting Information), we calculated LODs for different microRNAs in buffer and it is 32 aM for microRNA-10b, while microRNAs with 18 (microRNA-p), 12 (microRNA-10a), and 4 (microRNA-q) base-pair mismatched display LODs of 5.2 fM, 0.15 pM, and 0.4 nM, respectively, see **Figure S1** and **Table-S3 and S4**. These results support our above-mentioned hypothesis that the LSPR sensitivity of our nanoplasmonic sensor decreases as the mismatch is closer to the surface of the TNPs, because when there is a mismatch, the wavefucntion of conduction electrons of TNPs are not able to delocalize throughout the duplex -ssDNA/microRNA structure. Thus, with mismatch the *width* of plasmon excitation does not increase (consider a Au TNP to be a plasmonic slab) as well as the aspect ratio (edge-length: thickness) of TNPs remains constant.[23] This plasmoelectronic phenomenon is discussed in more detail below.

Most strikingly, microRNA-r in which the first three nucleotides are completely missing from the 3' end but is fully complementary to -ssDNA-10b for the remaining 20 nucleotides does not display any observable $\Delta\lambda_{LSPR}$ values. The same nanoplasmonic sensor was then treated with RNaseH enzyme to regenerate the sensor[15, 24] and incubated in 1.0 nM solution of microRNA-10b. We observe ~10 nm $\Delta\lambda_{LSPR}$ shifts, suggesting appropriate sensitivity and selectivity of the sensors (**Figure 2B**). If the underlying physical property of greatest significance was the change in local dielectric environment of nanoprisms, we would expect a large influence on LSPR-properties when microRNA-r formed its duplex with the LSPR-sensor (-ssDNA-10b) and would expect it to induce a large λ_{LSPR} red-shift. The attachment of microRNA-r to the sensor was confirmed by fluorescence study described below. The experimental data are remarkable and suggest that our sensing mechanism is most likely controlled by the delocalization of conduction electrons wavefunction and an increase in the slab height rather than the influence of dielectric change, which is the traditionally accepted theory of LSPR-based detection and quantification (assay) of biomolecules.[19, 20, 25] Taken together, the specific physicochemical property of the microRNA enabling delocalization of conduction electron wavefunctions through coupled -ssDNA/microRNA duplex leading to the zM sensitivity reported.

A single base-pair match in short –ssDNA/microRNA duplex should not influence their binding constant significantly.[26] Furthermore, long incubation time of our sensors in the microRNA solution should allow all the microRNAs are to be attached on the sensors regardless of their nucleic acid sequence. One could, however argue that the observed $\Delta\lambda_{LSPR}$ values for different mismatches are due to the variable number of microRNAs that are attach onto the nanoplasmonic sensor, and thus the change in local dielectric environment varies between them. We overruled such an argument by quantifying sensor-bound microRNAs using fluorescence spectroscopy. MicroRNAs were labeled at 5'

end with fluorescein amidite (FAM). Nanoplasmonic sensors were prepared with –S$(CH_2)_6$-ssDNA-10b and then incubated in 1.0 nM FAM-labeled microRNA solution, allowed to hybridized overnight and then each sensor was washed to remove loosely bound microRNAs. Finally, –S$(CH_2)_6$-ssDNA-10b/microRNA duplex was released in solution through ligand exchange reaction (see Supporting Information for detailed experimental procedure).[17, 27] **Figure 2C** shows photoluminescence (PL) spectra for each microRNA listed in **Figure 1C** in which characteristic PL peak of FAM ~525 nm is observed. *Noticeably, PL peak intensity for different microRNA is within the experimental error*. This result is significant because it suggests that the number of microRNA attached to the sensors is identical irrespective to single base-pair mismatch at different locations in the duplex. Moreover, the refractive index for microRNA-10b, -10a, -p, and -q should be nearly identical. Therefore, change in the local dielectric environment of TNPs in the presence of different microRNAs is presumably similar and should provide similar $\Delta\lambda_{LSPR}$ values, as opposed to our experimental data (see **Figure 2A**). Based on the LSPR and PL data for different microRNAs, we alternatively suggest that the unprecedentedly high sensitivity of our nanoplasmonic sensors for detection of microRNAs arises from the increase of confinement box size of Au TNPs through wavefunction delocalization that substantially affects their aspect ratios (edge-length: thickness of a TNP) and LSPR properties, and thus provides a new plasmoelectronic phenomenon that has not been demonstrated before with respect to the characterization of LSPR-based transduction mechanisms for assaying short nucleotides.

In fact, our above-mentioned experimental data provide a guideline for the surface plasmon excitation delocalization-based sensing mechanism: (i) a fully complementary nucleotide sequence is required for extended delocalization of conduction electron wavefunctions throughout the entire -ssDNA/microRNA duplex and (ii) this transduction mechanism is not controlled by the specific identity of nucleotide in the –ssDNA/microRNA

duplex. To investigate this further, we turned to microRNA-182, which contains an entirely different nucleotide sequence than microRNA-10b (**Table S1 and S2**). There are 22 nucleotides in microRNA-182 as opposed to 23 in microRNA-10b, thus a slightly higher delocalization is expected in the latter case. Secondly, microRNA-182 - an oncogenic microRNA that promotes the metastatic process of bladder cancer - can be used as a biomarker for early detection of BC.[28] We prepared our nanoplasmonic sensor by attaching –$S(CH_2)_6$-ssDNA-182 on Au TNPs, and then incubated it in 1.0 nM microRNA-182 solution. We observe LSPR red-shifts in the UV-visible absorption spectrum with an $\Delta\lambda_{LSPR}$ value of 7.2 nm (see **Figure S2**). As shown in **Figure 2D**, the LOD for fully complementary microRNA-182 is 82 aM, which is nearly 2.5-fold lower than that of microRNA-10b. We believe this is related to the overall length of -ssDNA/microRNA duplex, which influences the extent of delocalization. Finally, nanoplasmonic sensors containing –$S(CH_2)_6$-ssDNA-182 were treated with single base-pair mismatch microRNA-s, -t, and v and the $\Delta\lambda_{LSPR}$ values and LODs (see **Table-S3 and S4, and Figure S3**) are in good agreement with the hypothesis of the wavefunctions delocalization process. Taken together, our experimental results show that the transduction mechanism does not depend on the chemical identity of nucleotide in the –ssDNA/microRNA duplex. Most importantly, the proposed plasmoelectronic phenomenon has allowed us to quantify short noncoding RNAs with a single nucleotide specificity.

In literature, both experimentally and theoretically have shown that the line-width (full-width at half maxima, FWHM) of LSPR peak of metal nanoparticles increases as the physical dimension (aspect ratio) of a nanoparticle increases.[19, 20, 29-31] In this context, it might be argued that upon conduction electron wavefunction delocalization, both height (thickness) and width (edge-length) of the plasmonic slab (e.g., Au TNP) would increase. One would also expect that the thiolated –ssDNAs

preferentially attach along the high-index facets, i.e., three sides, edges, and sharp tips of a TNP as compared to the planner top surface. Therefore, TNPs grow more along the edges than the height, and thus increases their overall aspect ratio. Together, the plasmoelectronic effect causes a difference in FWHM (ΔFWHM: before - after microRNA attachment) depending on the extent of delocalization and increase in aspect ratio that are controlled by the location of the base-pair mismatch in -ssDNA/microRNA duplex (**see Figure 1A**) that elucidate the delocalization mechanism. **Figure 2E and Figure S4** illustrate the LSPR extinction spectra of -S$(CH_2)_6$-ssDNA-10b-functionalized nanoplasmonic sensors in the presence of different microRNAs with a single base-pair mismatch. Indeed, an increase in ΔFWHM of LSPR dipole peak of Au TNP is observed from 4th to 12th to 18th positions mismatch in -ssDNA-10b/microRNA duplex (see **Figure 2F**). The largest ΔFWHM of 16 nm is observed for the fully complementary -ssDNA-10b/microRNA-10b duplex. Although our PL analysis unequivocally supports the attachment of microRNA-r to nanoplasmonic sensors, no noticeable differences in ΔFWHM are observed. Therefore, the higher the delocalization, the greater the confinement box size, and consequently the larger the ΔFWHM value.

The Role of Linker Between Au TNP and -ssDNA on Conduction Electron Wavefunction Delocalization. To improve the delocalization of conduction electron wavefunctions of Au TNPs into -ssDNA/microRNA duplex it is necessary to reduce the insulating barrier between the TNP and the duplex. For the study described above, we used a –$(CH_2)_6$ linker to attach -ssDNA-10b (182) onto TNPs and to prepare nanoplasmonic sensors. The presence of the linker is absolutely necessary to create homogeneous packing of -ssDNAs onto the surface of the TNPs and avoid their coiling.[12, 13] We believe that the shorter alkyl chain length creates a thinner insulating barrier and increases the conduction electron wavefunction delocalization into the -ssDNA/microRNA duplex, which results in a larger shift in $\Delta\lambda_{LSPR}$ and higher sensitivity. To test this, we varied the linker chain length from -

$(CH_2)_3$ to $-(CH_2)_9$, see **Figure 1A**. We used -ssDNA-10b as a model receptor for microRNA-10b quantification in PBS buffer, while keeping other parameters in nanoplasmonic sensor fabrication identical. **Figure 3A** illustrates the average $\Delta\lambda_{LSPR}$ values for three different linkers as a function of microRNA-10b concentration. The LODs for $-(CH_2)_3$ and $-(CH_2)_9$ are 137 zeptomolar (zM) and 0.81 pM, respectively (see **Table-S5 and S6, and Figure S5**). We also attached a $-(CH_2)_{16}$ linker but no noticeable $\Delta\lambda_{LSPR}$ is observed (data not shown). Strikingly, the sensitivity of our nanoplasmonic sensors constructed with $-S(CH_2)_3$-ssDNA-10b is nearly 240-fold higher than that of $-S(CH_2)_6$-ssDNA-10b. Only recently, nanoplasmonic sensors consisting of Au-Ag core-shell nanocubes and tetrahedral structured DNA was used for microRNA quantification at aM concentration range using a single nanoparticle scattering measurement.[32] Nevertheless, we conclude that unprecedentedly high sensitivity of our nanoplasmonic sensors constructed with $-(CH_2)_3$-ssDNA-10b arises due to improved delocalization of conduction electrons wavefunction of Au TNPS into -ssDNA/microRNA duplex by reducing the insulating barrier between the TNP and duplex. Finally, we observe the highest (21 nm) and lowest (10 nm) ΔFWHM values for $-(CH_2)_3$ and $-(CH_2)_9$ linker, respectively (**Figure 3B and Figure S6**). This trend also supports our surface plasmon excitation delocalization mechanism. We should mention that at 500 zM detection limit, ~3000 microRNAs would present in 10 mL solution. A typical size of our nanoplasmonic sensors is 25 x5 mm^2 (1.25 $x10^{14}$ nm^2), and we calculated that ~12% of the substrate was covered with TNPs (ca. 2.0 x 10^{10} TNP). In this context, the probability of microRNA attachment to each TNP is exceedingly low. The area of a sensor exposed to Xenon flash lamp light of the UV-visible spectrophotometer was determined to be 1.96 x 10^{13} nm^2. Therefore, nearly an entire nanoplasmonic sensor resides within the path of the light beam that allows quantification of ~3000 microRNAs in order to obtain a limit of detection of 500 zM.

Mechanistic Understanding of Surface Plasmon Excitation Delocalization-Driven Plasmoelectronic Phenomenon. The plasmonic slab model proposed by Govorov et al.[23] suggests that a large number of highly excited electrons can be generated for a slab of 8 nm (the height of our Au TNPs) when Fermi gas is perturbed upon light excitation. These excited electrons can be used for various catalytic transformations where electrons are transferred from plasmonic nanoparticles to their surroundings and holes are neutralized by using scavenger. In contrast, photoexcited electrons have the ability to delocalize their wavefunctions into the immediate surrounding such as to a ligand environment. Therefore, the confinement box size (also aspect ratio of TNPs) increases that results in red shifting of the LSPR peak. We refer to this plasmoelectronic effect as surface plasmon excitation delocalization. Most important, this plasmoelectronic effect should be reversible by disrupting the delocalization process. Recently, we[33, 34] and others[35] have demonstrated reversible electron wavefunction delocalization of CdSe quantum dots and manipulated their optoelectronic properties. This delocalization mechanism, which should be applicable to plasmonic nanoparticles under light excitation, however has not been explored in metal nanoparticles yet. Based on the experimental data, we propose **Figure 4** as the possible mechanism for light-induced plasmoelectronic phenomenon of -ssDNA-functionalized Au TNPs. Here, highly pi-stacked -ssDNA/microRNA duplexes facilitate electron wavefunction delocalization which results in an increase in dimension of the plasmonic slab. In this context, as the delocalization improves, the aspect ratio of TNPs becomes higher, which results in more red-shifting of the LSPR peak. Therefore, the electronic dimensions such as edge-length and height of Au TNP are higher than the physical dimension of 42 and 8 nm of edge-length and height, respectively.[16, 36] Most importantly, electron delocalization through the phosphate backbone of DNA could take place in attosecond time-scale[37] and thus, delocalization is highly feasible under our experimental condition where continuous wave plasmonic excitation is performed during the steady-state extinction measurements. Nevertheless, precise determination of the increase of electronic

dimension (plasmonic slab) of our nanoplasmonic sensors requires sophisticated mathematical calculations, beyond our expertise. We should mention that the electron wavefunction delocalization mechanism is different than DNA-mediated charge transport (CT) process, as discussed below.

Long distance CT through a duplex DNA backbone has been known for more than two decades,[38, 39] where a single base pair mismatch can disrupt the electron flow and influence the conductivity significantly.[40, 41] Thus, DNA can be considered a molecular nanowire consisting of multiple highest occupied (HOMO) and lowest unoccupied (LUMO) molecular orbitals, which facilitate the CT process and charge delocalization.[42] Electron donors such as CdSe quantum dots[43] and Au[44] nanoparticles can transfer charge to MOs of DNA that transport through DNA nanowires up to several micrometers. However, LSPR (photo-excited conduction electrons) supports the escape of conduction electrons from metallic nanoparticles in the solid-state, influencing their optical properties, and causing a *permanent* electron-based damage of the local dielectric environment of nanoparticles. In other words, if CT were the basis for the observed phenomenon, the LSPR properties would not be able to be restored. [44] In contrast, our nanoplasmonic microRNA sensors show excellent regeneration by enzymatic cleaving of –ssDNA/microRNA duplex and re-hybridization of the sensors in microRNA solution for 5 consecutive days.[15, 24] Therefore, we believe delocalization of conduction electrons wavefunction into hybrid MOs (LUMOs') (see **Figure 4**, yellow wavy line) is occurring and not the transfer of conduction electrons that would permanently change the LSPR-properties of Au TNPs, and over time would destroy TNPs because of the building of excess positive charge (hole).

We believe that metallic nanostructures should be highly LSPR responsive upon delocalization of exciton wavefunctions (plasmoelectronic effects) and minute change in their aspect ratio. Au TNPs, although display strong LSPR response when small changes occur either in their surrounding medium refractive index or aspect ratios because of their strong electromagnetic (EM) field enhancement, one

would also expect to observe the plasmoelectronic effects for other anisotropically-shaped nanostructures such as nanorods and nanostars because they also display strong EM-field enhancements. It is therefore imperative to investigate shape and composition (e.g., Ag TNPs) dependent plasmoelectronic effects of nanostructures and their ability towards ultrasensitive biosensing, a current research focus of our laboratory.

Liquid Biopsy to Identify More Specific Biomarkers for Early Diagnostic of Bladder Cancer. MicroRNAs are small non-protein-coding RNAs that have been shown to control cell growth, differentiation and apoptosis, and thus variable microRNA expressions are linked to tumorigenesis.[45] Because of their unusually high stability in human biofluids such as serum and plasma, circulating microRNAs have the unmatched potential to serve as diagnostic markers for cancer for development of a liquid biopsy with unmatched potential to detect cancer faster and much earlier than currently available technology. There are two different types of microRNAs of interest in cancer screening: (i) Oncogenic, which promote tumor development by inhibiting tumor suppressor genes that control either cell differentiation or apoptosis. Oncogenic microRNAs are overexpressed in different cancer including BC. (ii) Tumor suppressors, which prevent tumor development by negatively inhibiting oncogenes that control either cell differentiation or apoptosis. The expression of tumor suppressor microRNAs is decreased in cancer cells.[45] Because tumor suppressor microRNAs levels decrease in cancer cells as compared to normal cells, it is extremely difficult to quantify them with a PCR-based assay, which is not very sensitive. Currently, there is no routine way to selectively detect and quantify (assay) circulating tumor suppressor microRNAs directly in crude human biofluids. Zeptomolar sensitivity of our nanoplasmonic sensors provides a unique advantage to assay both oncogenic and tumor suppressor microRNAs directly in unmodified plasma samples. Here, we present the first label-free assay to compare both oncogenic and tumor suppressor levels between patients with metastatic (MT, $n = 7$), non-metastatic (NMT, $n = 4$) and normal controls (NC, $n = 4$) from crude plasma.

The current FDA-approved urine cytology test shows poor sensitivity for low-grade lesions and significant disparity in specificity for different BC grades, thus it is a highly unreliable screening test. Biologically it is reported that microRNA-10b and -182 are upregulated, and microRNA-143 and -145 are downregulated in BC, therefore they could serve as alternative and more specific biomarkers for early diagnosis of BC.[28, 46-48] **Figure 5A-D** shows the concentration of these four microRNAs determined using our nanoplasmonic sensors directly from unmodified patient plasma utilizing the calibration plots developed in human plasma (**Figure S7)**. All seven MT patient samples show high levels of microRNA-10b (**Figure 5A**). Moreover, the levels of NC and NMT patient samples are 8- and 2-fold lower, respectively, as compared to MT samples. The results suggest that the microRNA-10b is not the most ideal biomarker for early diagnosis of BC ($p < 0.05$), but it is suitable to differentiate between MT and NMT disease stages ($p < 0.0001$). MicroRNA-182, however appears to be a less specific biomarker not only for early diagnosis of BC but also in cancer progression stages (**Figure 5B**). Strikingly, microRNA-143 and -145 levels differ by nearly 3- and 4.0 $x10^3$-fold between NC vs. NMT, and NMT vs. MT BC patient samples, respectively ($p < 0.0001$), see **Figure 5C and D**. Moreover, the difference between NC vs. MT is >1.0 x 10^4-fold for tumor suppressor microRNAs, in contrast to the ~6-fold difference observed for oncogenic microRNAs for the same patient samples. To further validate the results, we performed specificity tests of the nanoplasmonic sensors. These tests unequivocally support a high level of specificity towards the target microRNAs without any false positive responses (selectivity). Supporting Information file provides experimental details and LSPR spectra associated with specificity and selectivity tests, see **Figure S8**. Taken together, microRNAs that our body produces naturally to protect unusual transformation of cellular pathways (tumor suppressor microRNAs) could be more specific biomarkers for early detection of BC and possibly other cancers as well.

CONCLUSIONS

In summary, we have fabricated a nanoplasmonic sensor, which is capable of assaying microRNAs at ultralow concentration levels from patient plasma. In particular, for the first time we show that tumor suppressor microRNAs are likely to be more specific biomarkers than oncogenic ones for early detection of BC. Based on the experimental results, we believe a new transduction mechanism (plasmoelectronic effect), consisting of delocalization of photo-excited conduction electrons wavefunction of TNP into hybrid LUMOs, is involved for enabling such an unprecedentedly high sensitivity for microRNA detection and quantification. Furthermore, by utilizing Au TNPs as electron donors and their unique LSPR properties as a transduction method, we could experimentally probe the electron wavefunction delocalization and/or CT properties of short DNA molecules. The process of designing a new class of ultrasensitive nanobioelectronic devices is the current research focus of our laboratory. Taken together, our findings suggest that an ultrasensitive nanoplasmonic sensor, in addition to being a novel liquid biopsy platform for the detection of circulating microRNAs in patient plasma, may aid in developing early-stage, low-volume diagnostic tests for a variety of diseases and analysis for a single cancer cell, to better understand tumor heterogeneity.

LIST OF FIGURES

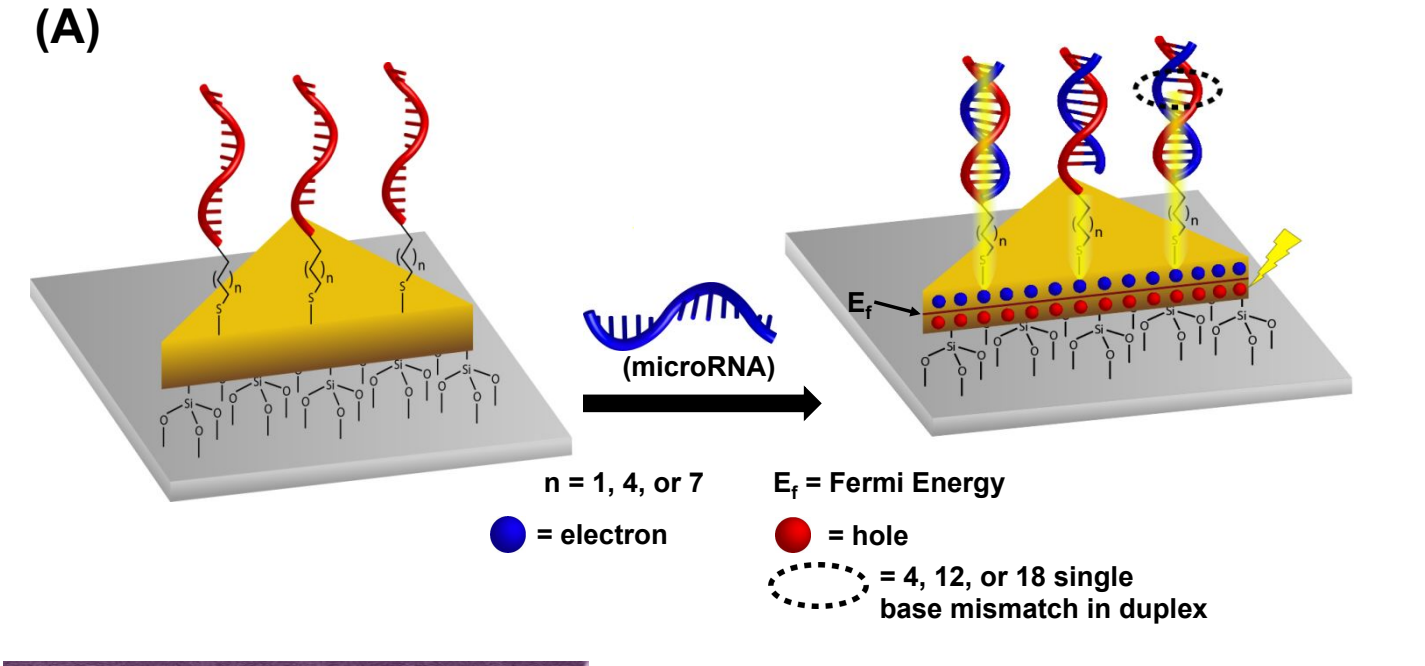

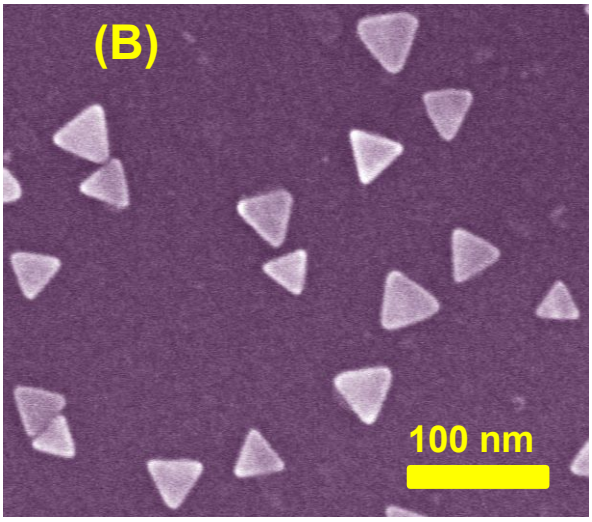

(C)

ssDNA-10b : 5'CACAAA TTCGGTT CT ACAGGGTA3'
microRNA-10b: 3'GUGUUUAAGCCAAGA UGUCCCAU5'
microRNA-p : 3'GUGUUUAAGCCAAGAUGGCCCAU5'
microRNA-10a: 3'GUGUUUAAGCCUAGAUGUCCCAU5'
microRNA-q : 3'GUGCUUAAGCCAAGAUGUCCCAU5'
microRNA-r : 3' UUUAAGCCAAGAUGUCCCAU5'

Figure 1. The structural parameters of nanoplasmonic sensors modulating the plasmoelectronic effects at the Au TNP and –S-ssDNA/microRNA interface. (A) Schematic representation of characterizing the delocalization of conduction electron wavefucntions of TNPs into -ssDNA/microRNA duplex. (Left panel): Au TNPs are chemically attached onto a silanized glass substrate and then their surface are functionalized with mixed HS-PEG: $HS(CH_2)_n$-ssDNA-X to prepare LSPR-based nanoplasmonic sensors. (Right panel): Incubation of sensors in microRNA solution results in formation of -ssDNA/microRNA duplex. Photo-excitation of TNP results in generation of localized surface plasmon. Wavefunction of conduction electrons (surface plasmon excitation) delocalizes into the -ssDNA/microRNA duplex (yellow shading) that is manipulated through single base-pair mismatch in the duplex and spacing [varying alkyl chain length, $-(CH_2)_n-$, n = 3, 6, and 9) between TNP surface and 5'-end of -ssDNA-10b ("linker"). For simplicity wavefunction delocalization

along the TNP edges and -S-PEG$_n$ (n = 4 and 6) spacer are not showing. The image is not to scale. **(B)** Scanning electron microscopy image of ~42 nm edge-length and ~8 nm height Au TNPs attached onto silanized glass substrate used for nanoplasmonic sensors fabrication. **(C)** Depiction of -ssDNA-10b and microRNA molecules used in the studies to investigate conduction electrons wavefunction delocalization. The red letters represent the position of the single base-pair mismatch in the duplex structure.

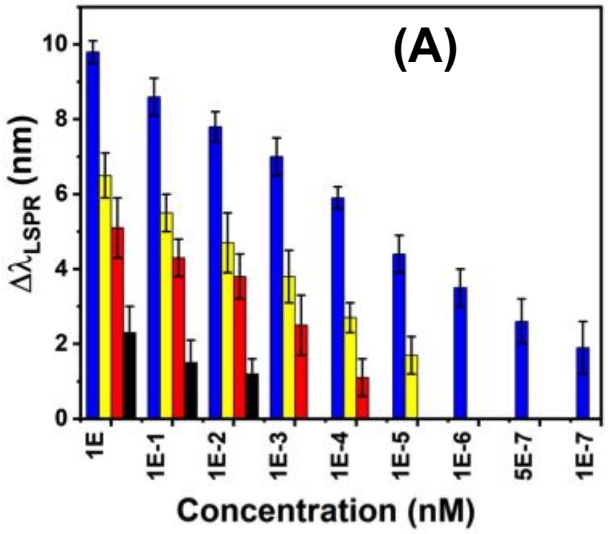

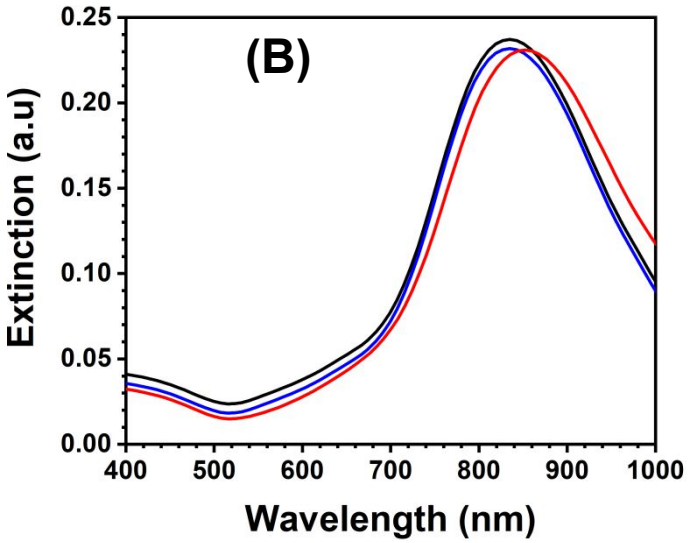

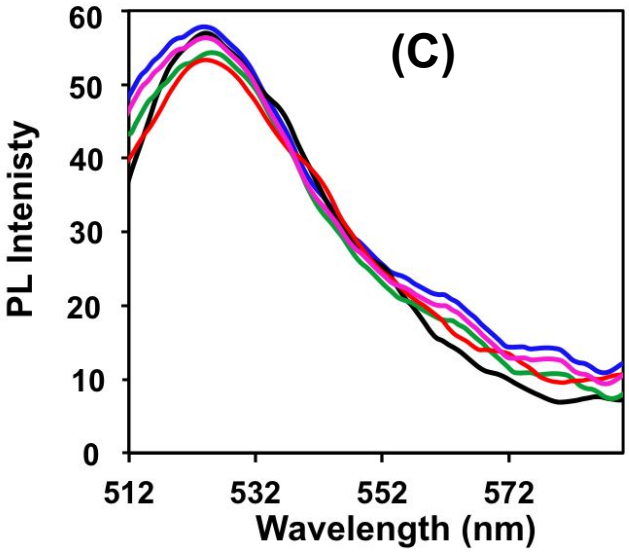

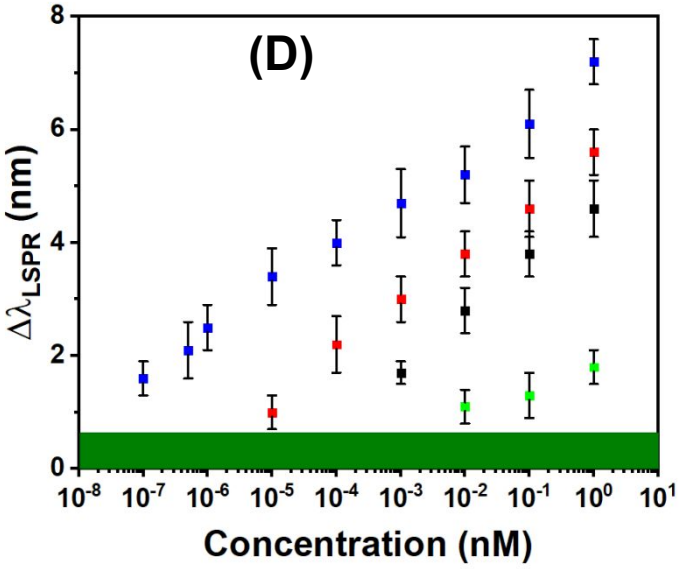

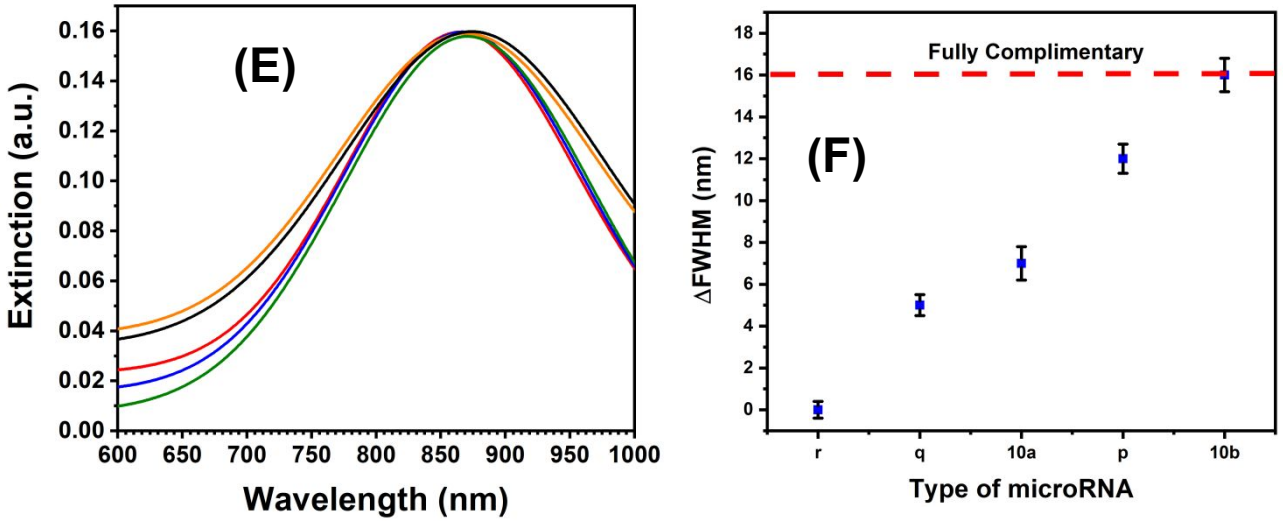

Figure 2. Spectroscopy characterization of surface plasmon excitation delocalization by manipulating the structural parameters of microRNAs. (A) Comparison of microRNA-10b (blue bars), microRNA-p (yellow bars), microRNA-10a (red bars), and microRNA-q (black bars) concentration dependent LSPR response in PBS buffer. For microRNA-r no detectable LSPR shift was observed. The sensors were constructed with mixed HS-PEG: $HS(CH_2)_6$-ssDNA-10b. **(B)** UV-visible extinction spectrum of nanoplasmonic sensors prepared with mixed HS-PEG: $HS(CH_2)_6$-ssDNA-10b (black curve), after incubation with 1.0 nM microRNA-r (blue curve), and then treatment with 15 units of RNase H for 2 h, and then incubation in 1.0 nM microRNA-10b solution (red curve). All the spectra were collected in PBS buffer. **(C)** Photoluminescence (PL) spectra of different microRNAs: microRNA-10b (red curve), microRNA-p (green curve), microRNA-10a (purple curve), microRNA-q (blue curve), and microRNA-r (black curve). For this study 5′ Fluorescein amidite (FAM) tagged microRNA were used. PL spectra were collected at 496 nm excitation wavelength. **(D)** Average $\Delta\lambda_{LSPR}$ value of nanoplasmonic sensors after incubation in different microRNAs of varying concentrations: microRNA-182 (blue squares), microRNA-s (red squares), microRNA-t (black squares), and microRNA-v (green squares). The sensors were constructed with mixed HS-PEG: $HS(CH_2)_6$-ssDNA-182**.** The standard deviation of the blank (6 measurements) was 0.25 nm and the green bar represents three times this value. Concentrations were plotted on the axis in log scale in order to investigate non-specific adsorption at a lower concentration range. **(E)** UV-visible extinction spectrum of nanoplasmonic sensors for different microRNAs at 1.0 nM concentration: microRNA-10b (black curve), microRNA-p (yellow curve), microRNA-10a

(green curve), and microRNA-q (blue curve). Red curve represents the LSPR spectrum of nanoplasmonic sensors. **(F)** Measured relative change in full-width at half maximum before and after microRNA (ΔFWHM) attachment from panel E for different microRNAs.

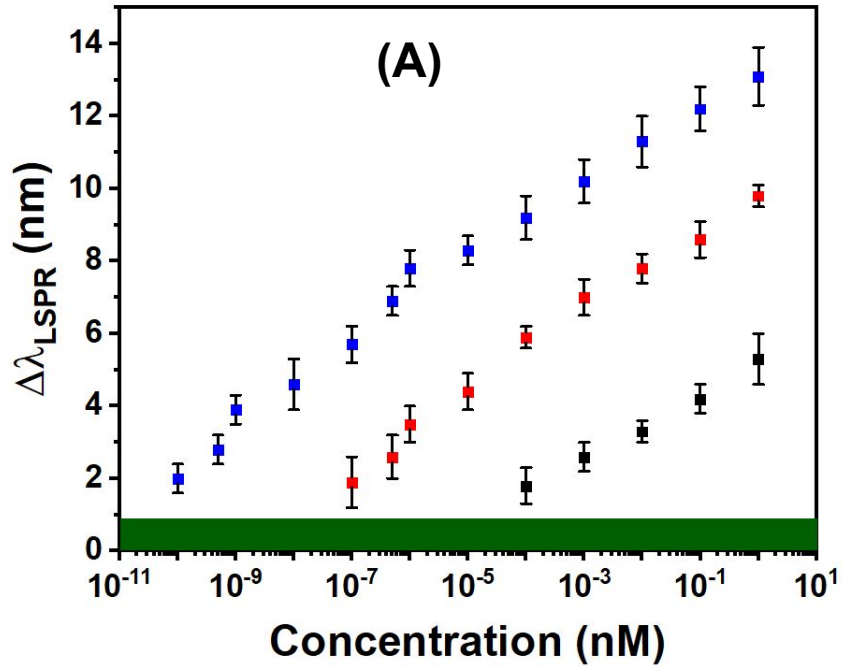

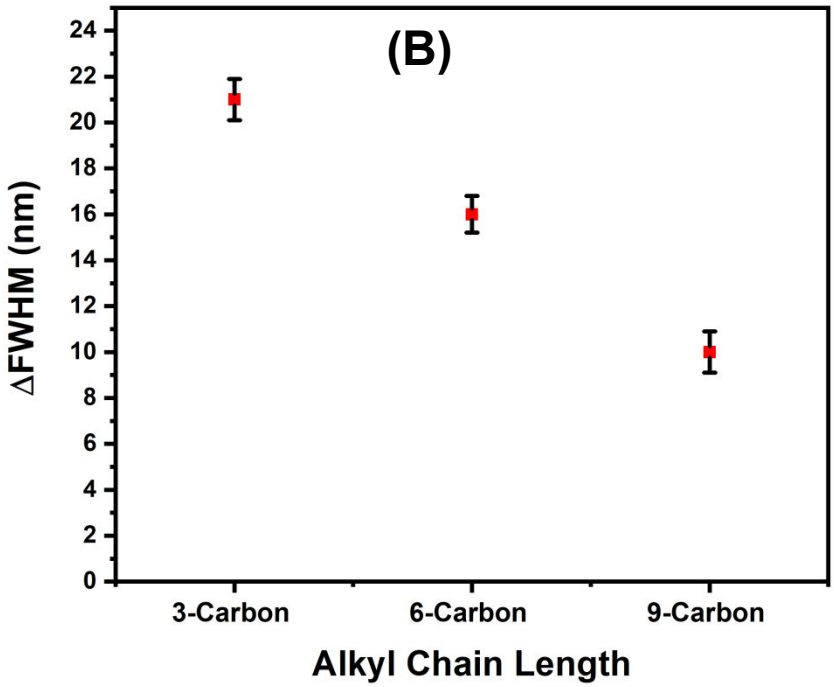

Figure 3. Characterization of the linker's role on conduction electron wavefunction delocalization. (A) Average $\Delta\lambda_{LSPR}$ value of nanoplasmonic sensors, which were prepared with three different spacers, -$(CH_2)_3$- (blue squares), -$(CH_2)_6$- (red squares), and -$(CH_2)_9$- (black squares) as a function of microRNA-10b concentration. Each spacer was connected with -ssDNA-10b as a recognition molecule for microRNA-10b. The standard deviation of the blank (6 measurements) was 0.32 nm and the green bar represents three times this value. Concentrations were plotted on the axis in log scale in order to investigate non-specific adsorption at a lower concentration range. (B) Measured FWHM for different alkyl chain length for 1.0 nM microRNA-10b concentrations.

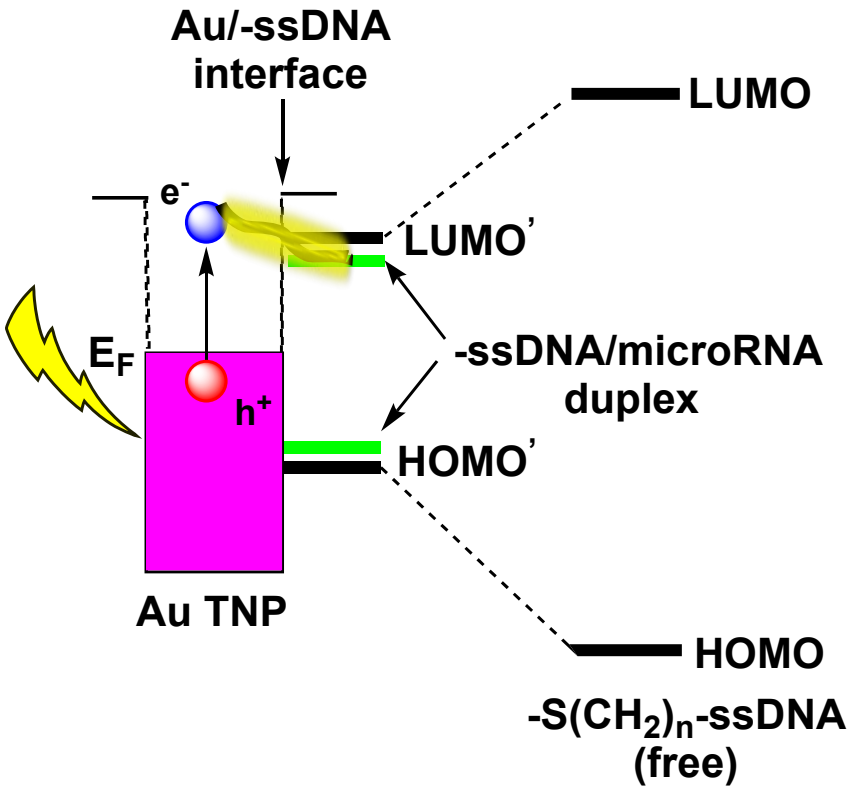

Figure 4. Schematic representation of proposed plasmon excitation delocalization at the Au TNP and –S(CH_2)$_n$-ssDNA/microRNA interface. Attachment of –S(CH_2)$_n$-ssDNA onto Au induces hybridization of electronic states and creates hybrid bonding (HOMO′) and antibonding (LUMO′) orbitals. The HOMO′-LUMO′ gap further reduces after formation of -ssDNA/microRNA duplex.[49] The LUMO′ further facilitates photo-excited conduction electron (blue dot, plasmon excitation) wavefunction delocalization (yellow wavy line) from Au TNP to the -ssDNA/microRNA moiety. The extended pi-stacking in –ssDNA/microRNA duplex facilitate the wavefunction delocalization. Delocalization expands the box size ("particle-in-a-box model) and increases the aspect ratio of TNP that together red-shifts the LSPR dipole peak. The image is not to scale.

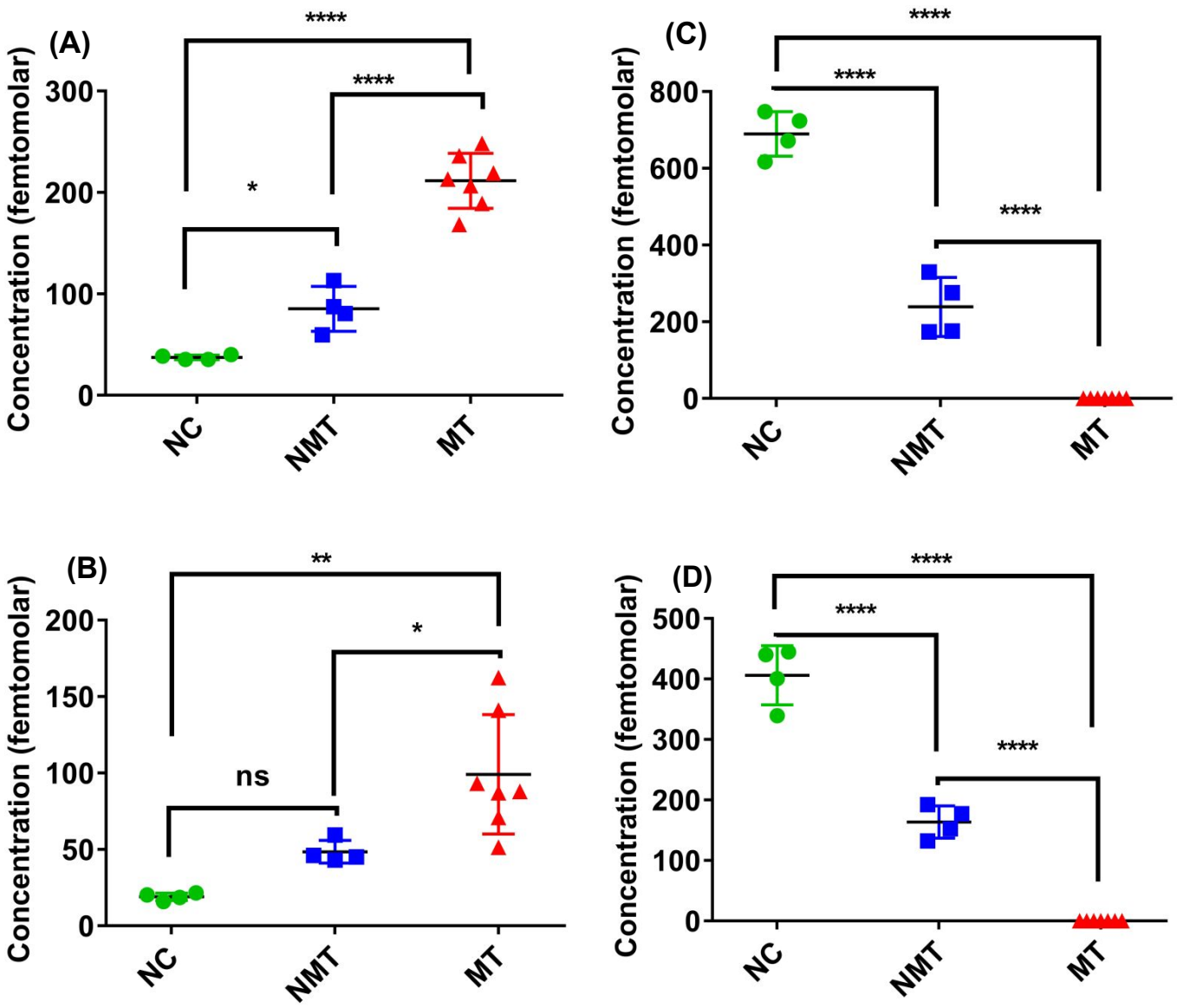

Figure 5. Statistical representation of microRNA analysis in bladder cancer (metastatic and nonmetastatic) patient plasma and normal control subjects. The concentration of oncogenic microRNAs (microRNA-10b and -182) and tumor suppressor microRNAs (microRNA-143 and -145) are determined in different stages of bladder cancer, non-metastasis (NMT) and metastasis (MT), as well as in healthy individuals (normal control, NC); n = 4 (NMT), n = 7 (MT), n = 4 (NC), two experiments for each sample (50 μL/sample) using our nanoplasmonic sensors. (**A**) microRNA-10b concentration in plasma. (**B**) Detection of microRNA-182 in plasma. (**C**) microRNA-143 concentration in plasma. **(D)** Detection of microRNA-145 in plasma. * P<0.05, **P <0.01, ****P<0.0001, and ns = not significant by one-way ANOVA.

ASSOCIATED CONTENT

Supporting Information. Additional information synthesis, instrumentation details, UV-visible absorption spectra showing specificity of the sensors, tables for nucleotide sequence, LSPR peak shift values, and limit of detection values for different mismatch. The following files are available free of charge. (PDF)

AUTHOR INFORMATION

Corresponding Author

*Rajesh Sardar; Email: rsardar@iupui.edu

Notes

Any additional relevant notes should be placed here.

ACKNOWLEDGMENT

The authors acknowledge financial support by the National Science Foundation under grant no. NSF CBET-1604617. The authors thank Dr. A Siegel (IUPUI) for helpful discussions, and Dr. S. Savant (IU Bloomington) for the guidance with statistical analysis of patient samples. H.O. thanks Newcastle University for Erasmus mobility award. We thank Claire Berman (IUPUI) for preparing the TOC graphic.

REFERENCES

1. Bartel, D. P. MicroRNAs: Genomics, Biogenesis, Mechanism, and Function. *Cell* **2004**, *116*, 281-297.
2. Esquela-Kerscher, A.; Slack, F. J. Oncomirs - microRNAs with a role in cancer. *Nat. Rev. Cancer* **2006**, *6*, 259-269.
3. Lockhart, D. J.; Winzeler, E. A. Genomics, gene expression and DNA arrays. *Nature* **2000**, *405*, 827-836.
4. Lu, J.; Getz, G.; Miska, E. A.; Alvarez-Saavedra, E.; Lamb, J.; Peck, D.; Sweet-Cordero, A.; Ebert, B. L.; Mak, R. H.; Ferrando, A. A., *et al.* MicroRNA expression profiles classify human cancers. *Nature* **2005**, *435*, 834-838.
5. Wang, J.; Chen, J.; Sen, S. MicroRNA as Biomarkers and Diagnostics. *J. Cell. Physiol.* **2016**, *231*, 25-30.
6. Petrocca, F.; Lieberman, J. Micromanipulating cancer: microRNA-based therapeutics? *RNA Biol.* **2009**, *6*, 335-340.
7. Qiu, L.; Zhang, W.; Tan, E. K.; Zeng, L. Deciphering the Function and Regulation of microRNAs in Alzheimer's Disease and Parkinson's Disease. *ACS Chem. Neurosci.* **2014**, *5*, 884-894.
8. Pandey, A. K.; Agarwal, P.; Kaur, K.; Datta, M. MicroRNAs in Diabetes: Tiny Players in Big Disease. *Cell. Physiol. Biochem.* **2009**, *23*, 221-232.
9. Creemers, E. E.; Tijsen, A. J.; Pinto, Y. M. Circulating MicroRNAs: Novel Biomarkers and Extracellular Communicators in Cardiovascular Disease? *Cir. Res.* **2012**, *110*, 483-495.
10. Rebecca, L. S.; Kimberly, D. M.; Ahmedin, J. Cancer statistics, 2018. *CA Cancer J Clin.* **2018**, *67*, 7-30.
11. Cissell, K. A.; Rahimi, Y.; Shrestha, S.; Hunt, E. A.; Deo, S. K. Bioluminescence-Based Detection of MicroRNA, miR21 in Breast Cancer Cells. *Anal. Chem.* **2008**, *80*, 2319-2325.
12. Johnson, B. N.; Mutharasan, R. Sample Preparation-Free, Real-Time Detection of microRNA in Human Serum Using Piezoelectric Cantilever Biosensors at Attomole Level. *Anal. Chem.* **2012**, *84*, 10426-10436.
13. Qavi, A. J.; Kindt, J. T.; Gleeson, M. A.; Bailey, R. C. Anti-DNA:RNA Antibodies and Silicon Photonic Microring Resonators: Increased Sensitivity for Multiplexed microRNA Detection. *Anal. Chem.* **2011**, *83*, 5949-5956.

14. Zhou, W.-J.; Chen, Y.; Corn, R. M. Ultrasensitive Microarray Detection of Short RNA Sequences with Enzymatically Modified Nanoparticles and Surface Plasmon Resonance Imaging Measurements. *Anal. Chem.* **2011**, *83*, 3897-3902.
15. Joshi, G. K.; Deitz-McElyea, S.; Liyanage, T.; Lawrence, K.; Mali, S.; Sardar, R.; Korc, M. Label-Free Nanoplasmonic-Based Short Noncoding RNA Sensing at Attomolar Concentrations Allows for Quantitative and Highly Specific Assay of MicroRNA-10b in Biological Fluids and Circulating Exosomes. *ACS Nano* **2015**, *9*, 11075-11089.
16. Joshi, G. K.; Blodgett, K. N.; Muhoberac, B. B.; Johnson, M. A.; Smith, K. A.; Sardar, R. Ultrasensitive Photoreversible Molecular Sensors of Azobenzene-Functionalized Plasmonic Nanoantennas. *Nano Lett.* **2014**, *14*, 532-540.
17. Guoke, W.; Jun, Y.; Jinliang, W.; Peng, G.; David, J. B.; Yu, C. Hairpin DNA-functionalized gold nanorods for mRNA detection in homogenous solution. *J. Biomed. Opt* **2016**, *21*, 97001-97009.
18. El-Sayed, M. A. Some Interesting Properties of Metals Confined in Time and Nanometer Space of Different Shapes. *Acc. Chem. Res.* **2001**, *34*, 257-264.
19. Willets, K. A.; Van Duyne, R. P. Localized Surface Plasmon Resonance Spectroscopy and Sensing. *Annu. Rev. Phys. Chem.* **2007**, *58*, 267-297.
20. Mayer, K. M.; Hafner, J. H. Localized Surface Plasmon Resonance Sensors. *Chem. Rev.* **2011**, *111*, 3828-3857.
21. Haes, A. J.; Chang, L.; Klein, W. L.; Van Duyne, R. P. Detection of a Biomarker for Alzheimer's Disease from Synthetic and Clinical Samples Using a Nanoscale Optical Biosensor. *J. Am. Chem. Soc.* **2005**, *127*, 2264-2271.
22. Mulvaney, P. Surface Plasmon Spectroscopy of Nanosized Metal Particles. *Langmuir* **1996**, *12*, 788-800.
23. Govorov, A. O.; Zhang, H.; Demir, H. V.; Gun'ko, Y. K. Photogeneration of hot plasmonic electrons with metal nanocrystals: Quantum description and potential applications. *Nano Today* **2014**, *9*, 85-101.
24. Joshi, G. K.; Deitz-McElyea, S.; Johnson, M.; Mali, S.; Korc, M.; Sardar, R. Highly Specific Plasmonic Biosensors for Ultrasensitive MicroRNA Detection in Plasma from Pancreatic Cancer Patients. *Nano Lett.* **2014**, *14*, 6955-6963.
25. Haes, A. J.; Van Duyne, R. P. A Nanoscale Optical Biosensor: Sensitivity and Selectivity of an Approach Based on the Localized Surface Plasmon Resonance Spectroscopy of Triangular Silver Nanoparticles. *J. Am. Chem. Soc.* **2002**, *124*, 10596-10604.
26. Cisse, I. I.; Kim, H.; Ha, T. A rule of seven in Watson-Crick base-pairing of mismatched sequences. *Nat. Struct. Mol. Biol.* **2012**, *19*, 623-627.
27. Demers, L. M.; Mirkin, C. A.; Mucic, R. C.; Reynolds, R. A.; Letsinger, R. L.; Elghanian, R.; Viswanadham, G. A Fluorescence-Based Method for Determining the Surface Coverage and Hybridization Efficiency of Thiol-Capped Oligonucleotides Bound to Gold Thin Films and Nanoparticles. *Anal. Chem.* **2000**, *72*, 5535-5541.
28. Proctor, I.; Stoeber, K.; Williams Gareth, H. Biomarkers in bladder cancer. *Histopathology* **2010**, *57*, 1-13.

29. Nusz, G. J.; Curry, A. C.; Marinakos, S. M.; Wax, A.; Chilkoti, A. Rational Selection of Gold Nanorod Geometry for Label-Free Plasmonic Biosensors. *ACS Nano* **2009**, *3*, 795-806.
30. Otte, M. A.; Sepulveda, B.; Ni, W.; Juste, J. P.; Liz-Marzan, L. M.; Lechuga, L. M. Identification of the Optimal Spectral Region for Plasmonic and Nanoplasmonic Sensing. *ACS Nano* **2009**, *4*, 349-357.
31. Mock, J. J.; Smith, D. R.; Schultz, S. Local Refractive Index Dependence of Plasmon Resonance Spectra from Individual Nanoparticles. *Nano Lett.* **2003**, *3*, 485-491.
32. Zhang, Y.; Shuai, Z.; Zhou, H.; Luo, Z.; Liu, B.; Zhang, Y.; Zhang, L.; Chen, S.; Chao, J.; Weng, L., *et al*. Single-Molecule Analysis of MicroRNA and Logic Operations Using a Smart Plasmonic Nanobiosensor. *J. Am. Chem. Soc.* **2018**, *140*, 3988-3993.
33. Lawrence, K. N.; Dutta, P.; Nagaraju, M.; Teunis, M. B.; Muhoberac, B. B.; Sardar, R. Dual Role of Electron-Accepting Metal-Carboxylate Ligands: Reversible Expansion of Exciton Delocalization and Passivation of Nonradiative Trap-States in Molecule-like CdSe Nanocrystals. *J. Am. Chem. Soc.* **2016**, *138*, 12813-12825.
34. Teunis, M. B.; Nagaraju, M.; Dutta, P.; Pu, J.; Muhoberac, B. B.; Sardar, R.; Agarwal, M. Elucidating the role of surface passivating ligand structural parameters in hole wave function delocalization in semiconductor cluster molecules. *Nanoscale* **2017**, *9*, 14127-14138.
35. Jin, S.; Harris, R. D.; Lau, B.; Aruda, K. O.; Amin, V. A.; Weiss, E. A. Enhanced Rate of Radiative Decay in CdSe Quantum Dots upon Adsorption of an Exciton-Delocalizing Ligand. *Nano Lett.* **2014**, *14*, 5323-5328.
36. Joshi, G. K.; Smith, K. A.; Johnson, M. A.; Sardar, R. Temperature-Controlled Reversible Localized Surface Plasmon Resonance Response of Polymer-Functionalized Gold Nanoprisms in the Solid State. *J. Phys. Chem. C* **2013**, *117*, 26228-26237.
37. Ikeura-Sekiguchi, H.; Sekiguchi, T. Attosecond Electron Delocalization in the Conduction Band

through the Phosphate Backbone of Genomic DNA. *Phys. Rev. Lett.* **2007**, *99*, 228102-228104.
38. Genereux, J. C.; Barton, J. K. Mechanisms for DNA Charge Transport. *Chem. Rev.* **2010**, *110*, 1642-1662.
39. Murphy, C. J.; Arkin, M. R.; Jenkins, Y.; Ghatlia, N. D.; Bossmann, S. H.; Turro, N. J.; Barton, J. K. Long-range photoinduced electron transfer through a DNA helix. *Science* **1993**, *262*, 1025-1029.
40. Hihath, J.; Xu, B.; Zhang, P.; Tao, N. Study of single-nucleotide polymorphisms by means of electrical conductance measurements. *Proc. Nat. Acad. Sci.* **2005**, *102*, 16979-16983.
41. Renaud, N.; Berlin, Y. A.; Ratner, M. A. Impact of a single base pair substitution on the charge transfer rate along short DNA hairpins. *Proc. Nat. Acad. Sci.* **2013**, *110*, 14867-14871.
42. Berlin, Y. A.; Burin, A. L.; Ratner, M. A. DNA as a molecular wire. *Superlattices and Microstructures* **2000**, *28*, 241-252.

43. Goodman, S. M.; Singh, V.; Ribot, J. C.; Chatterjee, A.; Nagpal, P. Multiple Energy Exciton Shelves in Quantum-Dot–DNA Nanobioelectronics. *J. Phys. Chem. Lett.* **2014**, *5*, 3909-3913.
44. Wirth, J.; Garwe, F.; Meyer, R.; Csáki, A.; Stranik, O.; Fritzsche, W. Plasmonically Enhanced Electron Escape from Gold Nanoparticles and Their Polarization-Dependent Excitation Transfer along DNA Nanowires. *Nano Lett.* **2014**, *14*, 3809-3816.
45. Zhang, B.; Pan, X.; Cobb, G. P.; Anderson, T. A. microRNAs as oncogenes and tumor suppressors. *Develop. Biol.* **2007**, *302*, 1-12.
46. Lin, T.; Dong, W.; Huang, J.; Pan, Q.; Fan, X.; Zhang, C.; Huang, L. MicroRNA-143 as a tumor suppressor for bladder cancer. *Journal of Urology (New York, NY, United States)* **2009**, *181*, 1372-1380.
47. Xiao, H.; Li, H.; Yu, G.; Xiao, W.; Hu, J.; Zeng, K. T. J.; He, W.; Zeng, G.; Ye, Z.; Xu, H. MicroRNA-10b promotes migration and invasion through KLF4 and HOXD10 in human bladder cancer. *Oncol. Rep.* **2014**, *31*, 1832-1838.
48. Kou, B.; Gao, Y.; Du, C.; Shi, Q.; Xu, S.; Wang, C.-Q.; Wang, X.; He, D.; Guo, P. miR-145 inhibits invasion of bladder cancer cells by targeting PAK1. *Urologic Oncology: Seminars and Original Investigations* **2014**, *32*, 846-854.
49. Rosu, F.; Gabelica, V.; De Pauw, E.; Antoine, R.; Broyer, M.; Dugourd, P. UV Spectroscopy of DNA Duplex and Quadruplex Structures in the Gas Phase. *J. Phys. Chem. A* **2012**, *116*, 5383-5391.

TOC Graphic

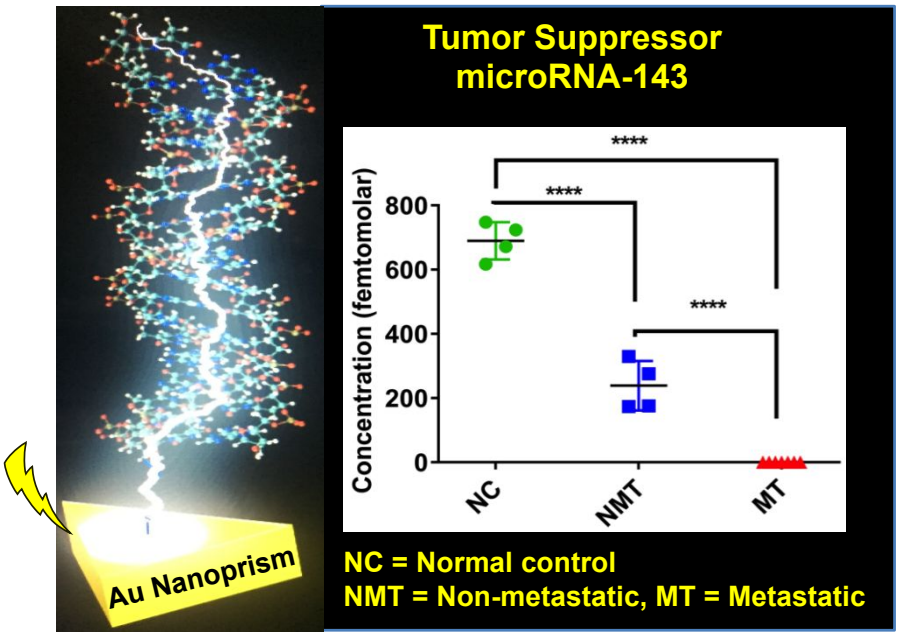
Tumor Suppressor
microRNA-143
Concentration (femtomolar)
800
600
400
200
0
****
****
****
NC
NMT
MT
Au Nanoprism
NC = Normal control
NMT = Non-metastatic, MT = Metastatic